NANO LETTERS
Cite This: Nano Lett. 2018, 18, 3630−3636
Letter
pubs.acs.org/NanoLett

Low-Frequency Current Fluctuations and Sliding of the Charge Density Waves in Two-Dimensional Materials

Guanxiong Liu,[†] Sergey Rumyantsev,[†,‡] Matthew A. Bloodgood,[§] Tina T. Salguero,[§] and Alexander A. Balandin*[,†]

[†]Nano-Device Laboratory (NDL) and Phonon Optimized Engineered Materials (POEM) Center, Department of Electrical and Computer Engineering, Materials Science and Engineering Program, University of California, Riverside, California 92521, United States

[‡]Ioffe Physical-Technical Institute, St. Petersburg 194021, Russia

[§]Department of Chemistry, University of Georgia, Athens, Georgia 30602, United States

Supporting Information

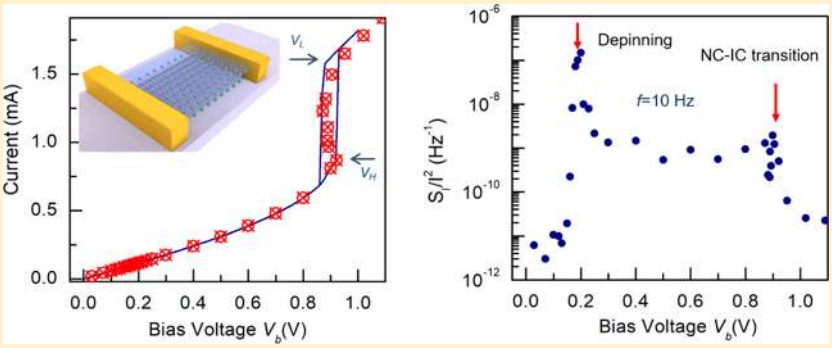

ABSTRACT: We investigated low-frequency noise in two-dimensional (2D) charge density wave (CDW) systems, 1*T*-TaS_2 thin films, as they were driven from the nearly commensurate (NC) to incommensurate (IC) CDW phases by voltage and temperature stimuli. This study revealed that noise in 1*T*-TaS_2 has two pronounced maxima at the bias voltages, which correspond to the onset of CDW sliding and the NC-to-IC phase transition. We observed unusual Lorentzian features and exceptionally strong noise dependence on electric bias and temperature, leading to the conclusion that electronic noise in 2D CDW systems has a unique physical origin different from known fundamental noise types. We argue that noise spectroscopy can serve as a useful tool for understanding electronic transport phenomena in 2D CDW materials characterized by coexistence of different phases and strong pinning.

KEYWORDS: *Charge density waves, depinning, low-frequency noise, two-dimensional, 1T-TaS_2*

The CDW phase is a macroscopic quantum state consisting of a periodic modulation of the electronic charge density accompanied by a periodic distortion of the atomic lattice.[1] The early work on CDW effects was performed with bulk samples, for example, TaS_3 or $NbSe_3$ crystals, which have quasi-one-dimensional (1D) crystal structures of strongly bound 1D atomic chains that are weakly bound together by van der Waals forces.[1−6] One of the most interesting phenomena observed in bulk quasi-1D CDW materials is the sliding of CDWs when the applied electric field exceeds a threshold value, E_{DT}, sufficient to depin the CDWs from defects.[1] CDW sliding leads to nonlinear direct current (dc) conductivity, "narrowband noise", which has the frequency, *f*, proportional to the current, *I*, and "broadband noise".[2−6] CDW sliding has been at the core of numerous device proposals.[1]

In recent years, there has been a rapid rebirth of interest in the physics of CDW effects with the focus on different types of materials, such as layered 2D crystals of 1*T*-TaS_2 and 1*T*-$TaSe_2$, which are members of the transition metal dichalcogenide (TMD) family. Unlike classical bulk CDW materials, these TMDs exhibit unusually high transition temperatures to different CDW symmetry-reducing phases.[7−14] The latter opens up the possibility of practical applications of CDW devices in communications and radiation-hard electronics.[13,15] The most interesting of these materials, 1*T*-TaS_2, undergoes a transition from the normal metallic phase to the incommensurate (IC) CDW phase at 545 K, then to the nearly commensurate (NC) CDW phase at 355 K, and finally to the commensurate (C) CDW phase at 180 K.[10−14] The NC-CDW phase consists of commensurate domains separated by regions that are incommensurate with the underlying crystal lattice. The transitions among CDW phases in 1*T*-TaS_2 films

Received: February 21, 2018
Revised: May 6, 2018
Published: May 16, 2018

DOI: 10.1021/acs.nanolett.8b00729
Nano Lett. 2018, 18, 3630−3636

can be affected by the number of layers as well as the applied field.[10,13] Despite the increasing attention to 2D CDW phenomena, there have been few reports on CDW depinning and sliding in 2D systems. Earlier attempts in finding the sliding effect in quasi-2D materials were not successful.[16] We are aware of just a couple of recent reports on CDW sliding in only one specific material system, quasi-2D rare-earth tritellurides,[17] and none on either "broadband" or "narrowband" noise of sliding CDWs in any of 2D systems.

In this Letter, we report on the low-frequency current fluctuations, that is, low-frequency noise (LFN), in a 2D CDW material system, 1*T*-TaS_2, considering both frequency and time-domain signals. This type of fluctuations, typically with the spectral density $S(f) \sim 1/f^{\gamma}$ ($\gamma \approx 1$), is found in almost all materials and devices.[18] It is conventionally known as $1/f$-noise in electronics, and it is often referred as "broadband" noise in the CDW field to distinguish it from "narrowband" noise.[1−6] Although practical applications can benefit from the reduction of LFN, it also can be used as an important metric that reveals information about the physical processes in materials.[19−21] Here we use LFN measurements to unambiguously observe the depinning and sliding of CDWs in the NC-CDW phase of 1*T*-TaS_2. Our results reveal unusual features in the LFN spectra of this quasi-2D CDW system, which are strikingly different from those in metals or semiconductors.

The high-quality 1*T*-TaS_2 two-terminal devices were fabricated from thin films, exfoliated from single crystals grown by the chemical vapor transport method (see Methods). The thickness of the thin films was ∼20 nm. The films were capped with *h*-BN to protect the 1*T*-TaS_2 channels from degradation.[13] The contacts were defined by electron beam lithography, resulting in devices with lateral dimensions of 1−3 μm by 0.8−1.5 μm. The edge contacts were fabricated by depositing metal after plasma etching through the *h*-BN capping layer. Figure 1a shows dc $I-V$ characteristics of a representative 1*T*-TaS_2 device at room temperature (RT). The CDW phase transition from NC to IC states is observed as an abrupt jump in the current and accompanying hysteresis, when the voltage exceeds the threshold voltages V_H and V_L. The NC to IC phase transition in 1*T*-TaS_2 has been studied in detail previously.[13] Whereas the NC−IC CDW transition is clearly visible in the $I-V$ curve, the depinning and onset of CDWs sliding is not obvious. From theoretical considerations one can deduce that somewhere before the hysteresis, where $I-V$ becomes superliner (e.g., regions I, II, or III), the collective current of the sliding CDW starts to contribute to the total current.[1] This feature is in striking contrast to the behavior of bulk quasi-1D CDW materials, which are characterized by an abrupt transition from the single-particle to the collective current.[1] This difference can be attributed to the fact that the quasi-2D NC-CDW phase consists of a mixture of C-CDW islands surrounded by the more strongly conducting IC-CDW phase.[10−13] As a result, the onset of sliding is overshadowed by conduction via the IC-CDW continuum.

The LFN measurements were conducted under dc bias voltages, V_b, increasing from 30 mV to 1.09 V, beyond the phase transition voltage (V_H = 0.92 V for this device). The dc bias points for each noise measurement are indicated by the red circles in Figure 1a. The normalized current-noise-spectral-density, S_I/I^2, versus V_b (f = 10 Hz), measured at RT, is presented in Figure 1b. One can see two well-resolved local maxima, which were reproducible for all studied devices. The first maximum at V_{DT} = 0.2 V indicates the depinning and onset

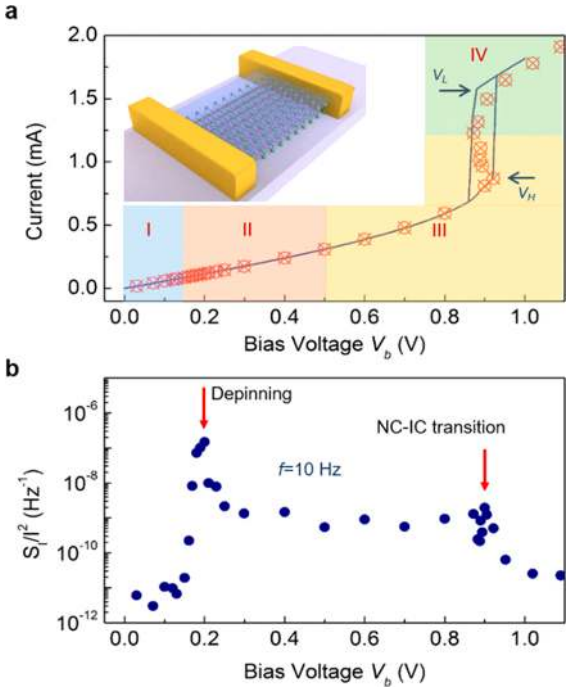

Figure 1. (a) $I-V$ characteristics of thin-film 1*T*-TaS_2 device at RT. The inset shows the device schematic. The abrupt NC−IC and IC-NC CDW phase transitions are seen at voltages V_H (up scan) and V_L (down scan). The red circles indicated the biasing points for LFN measurements. The biasing conditions are divided into four sections I, II, III, and IV. (b) Plot of S_I/I^2 at 10 Hz as a function of the bias voltage, V_b. Two pronounced local maxima correspond to the depinning and NC−IC phase transition.

of CDW sliding, whereas the second marks the NC−IC phase transition. The voltage, V_{DT}, corresponds to the threshold field of E_{DT} = 1.3 kV/cm for this device, a value that is four orders-of-magnitude larger than that in typical bulk quasi-1D CDW materials.[1] Considering that $E_{DT} \sim A^{-1/2}$ (A is the cross-section area),[1] we conclude that the large threshold field in quasi-2D materials is likely related to CDW pinning to the top and bottom surfaces. The depinning of CDWs in bulk classical quasi-1D materials is known to be accompanied by the superliner $I-V$ characteristic.[4] A weak nonlinearity is seen in Figure 1a. The derivative of this characteristic is provided in the Supporting Information Figure S2b. One can see that the onset of nonlinearity at $V > 0.1$ V is at the same voltage where the noise starts to grow rapidly (Figure 1b). Comparison of the noise data with $I-V$s and dI/dV characteristics confirms that LFN is an unambiguous metric for CDW sliding in 2D CDW materials.

Figure 2a−d shows S_I/I^2 versus f for four different biasing regions, marked as I, II, III, and IV in Figure 1a. At the small bias, $V_b \leq 150$ mV, S_I/I^2 follows typical $1/f$ dependence ($\gamma \approx 1$) as seen in Figure 2a. When V_b increases above 150 mV, the noise level increases sharply, and an excess noise with $\gamma = 2$ appears at the lower frequency range. As V_b increases further, the noise spectrum evolves into a Lorentzian shape, $S_I(f) = S_0 \times f_c^2/(f_c^2 + f^2)$, where $f_c = (2\pi\tau)^{-1}$ is the corner frequency, S_0 is the frequency-independent portion of $S_I(f)$ observed at $f < f_c$, and τ is the characteristic time of the fluctuation process.[22] In a very narrow bias range from 130 to 180 mV, the LFN level increases by four orders-of-magnitude. This fast growth of LFN is a signature of CDW depinning.[2−6] Even more interestingly, f_c

DOI: 10.1021/acs.nanolett.8b00729
Nano Lett. 2018, 18, 3630−3636

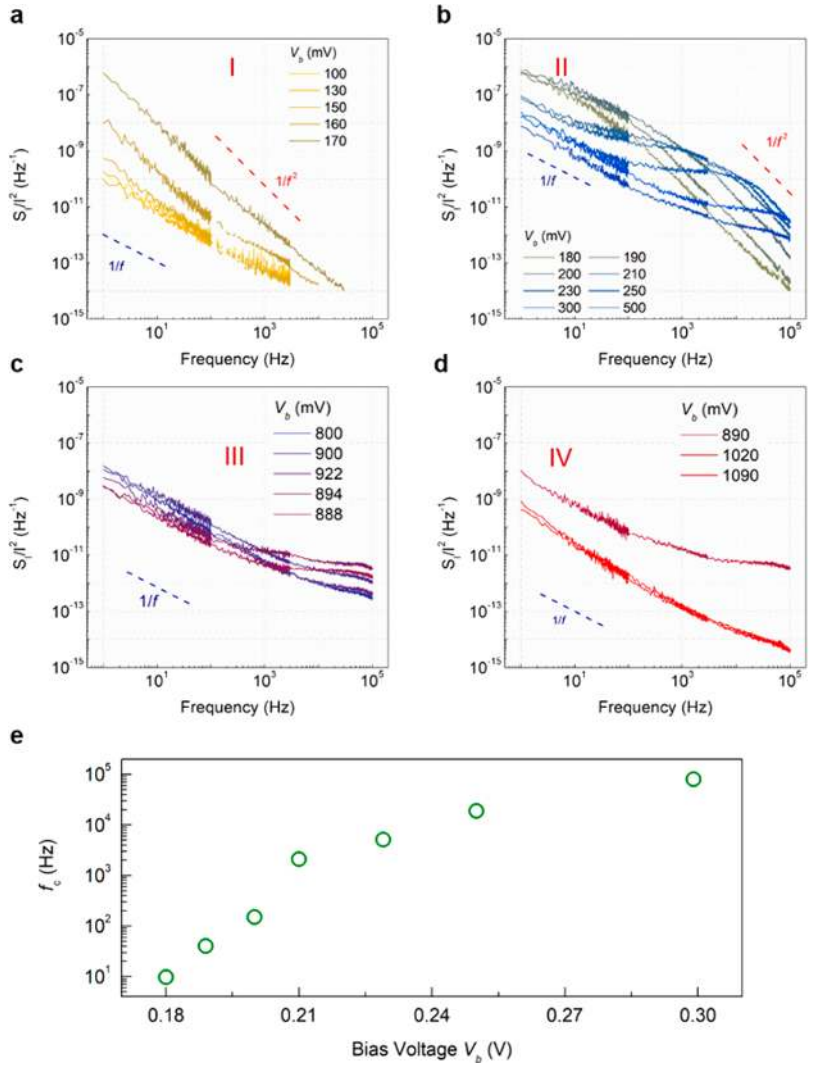

Figure 2. (a) S_I/I^2 for the bias region I. Below V_b = 150 mV, the noise is of $1/f$ type. Above 150 mV, the noise spectrum starts to change to $1/f^2$ type, which is indicative of the Lorentzian "tail". (b) S_I/I^2 for the bias region II. At V_b = 180 mV, the noise spectrum evolves into a Lorentzian shape with a corner frequency f_c = 10 Hz. As V_b increases, f_c shifts to 80.5 kHz at 300 mV. Above V_b = 300 mV, f_c stops moving to higher frequencies. (c) S_I/I^2 for the bias region III. The noise level reaches its maximum at the NC−IC point. (d), S_I/I^2 for the bias region IV. As V_b drives the 1*T*-TaS_2 into the IC-CDW phase, the noise level reduces and its shape returns to $1/f$ type. (e) The corner frequency f_c as a function of bias voltage V_b.

shifts upward with increasing bias, V_b (see Figure 2b). As V_b approaches the NC−IC phase transition voltage V_H, the overall noise magnitude attains its second local maximum. This behavior is expected because the domains of the superstructure in the NC phase are experiencing a drastic lattice reconstruction and melting into the IC phase. Inside the hysteresis window (shown in Figure 1a), $S_I(f)$ keeps almost the same shape with only small magnitude variations (Figure 2c). When V_b drives the transition to the IC-CDW phase, the noise decreases sharply, and the spectrum regains the $1/f$ dependence typical for metals (Figure 2d). A sharp increase of noise near and at the phase transition, known for other materials,[23,24] can be associated with abrupt changes in the resistance and instability of the phase transition. The strong dependence of noise on V_b in the regions where there are small changes in $I-V$ is more intriguing. Both the noise amplitude and spectrum shape change drastically with a very small change in V_b in region II (Figure 2a−d). The dependence of f_c on V_b for the region of the sliding CDW (region in II in Figure 1a) is summarized in Figure 2e. A voltage increase of only 120 mV results in a four orders-of-magnitude change in f_c. This drastic change in f_c with the bias is highly unusual for conventional materials, where a Lorentzian spectrum is associated with the generation-recombination (G-R) noise with f_c independent from the bias.[22] Therefore, the nature of the Lorentzian-type spectra in Figure 2 is different from the conventional G-R mechanism.

To elucidate the relative effects of electric field, E, and temperature, T, on CDW sliding in 2D systems, we performed noise measurement for T ranging from 290 to 375 K covering the NC−IC phase transition. The experiments were conducted at two bias voltages V_b = 30 mV and V_b = 60 mV with one less than V_{DT} and another greater than V_{DT} (V_{DT} = 50 mV). The temperature of the NC−IC phase transition, T = 355 K, is the same for these two voltages (Figure 3). The coincidence of the phase-transition temperatures indicates that Joule heating is negligible at these small biases.

The color map in Figure 4a shows the evolution of $S_I/I^2 \times f$, with temperature and frequency at fixed V_b= 30 mV. Below 320 K, the noise is of $1/f-$ type and the magnitude of $S_I/I^2 \times f$

DOI: 10.1021/acs.nanolett.8b00729
Nano Lett. 2018, 18, 3630−3636

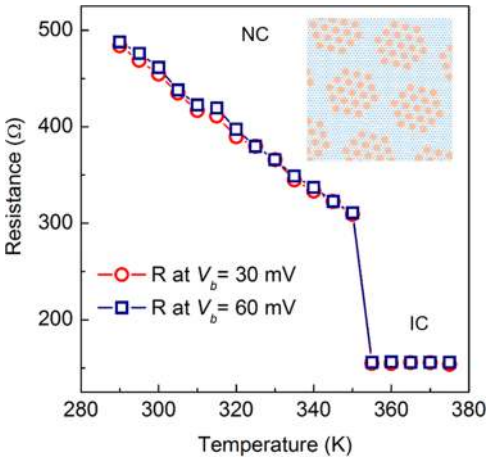

Figure 3. The resistance of 1*T*-TaS_2 device as a function of temperature. The NC−IC phase transition is attained at the same T = 355 K for both biases. The inset shows the domain structure of the NC-CDW phase.

is small (blue color). At $T \approx 325$ K, noise increases sharply, accompanied by a Lorentzian bulge with f_c = 52 Hz (red color). As T increases from 325 to 375 K, f_c remains almost constant (black arrow). Figure 4b shows the temperature-dependent noise profile at f = 10 Hz. The noise level increases by four orders-of-magnitude at 325 K followed by a slow increase with increasing temperature toward the NC−IC phase transition. Upon entering the metallic-like IC phase, the noise decreases by one order-of-magnitude and continues to decrease with T. Temperature alone cannot change f_c at the voltage below V_{DT}. In contrast, evolution of the Lorentzian bulge is completely different under the bias exceeding V_{DT}. Figure 4c shows the color map of $S_I/I^2 \times f$ at V_b = 60 mV. The corresponding profile is presented in Figure 4d. From ∼840 Hz at 290 K to ∼74 kHz at 315 K, f_c increases quickly with temperature. At temperatures nearing the NC−IC phase transition, f_c becomes undetectable. Above the NC−IC transition, the noise decreases and returns to $1/f$ type.

The evolution of f_c with temperature at two biases is summarized in Figure 5. Only in the case of $V_b > V_{DT}$ does the Lorentzian corner frequency f_c change with temperature. We further verified that f_c shifting was driven primarily by the

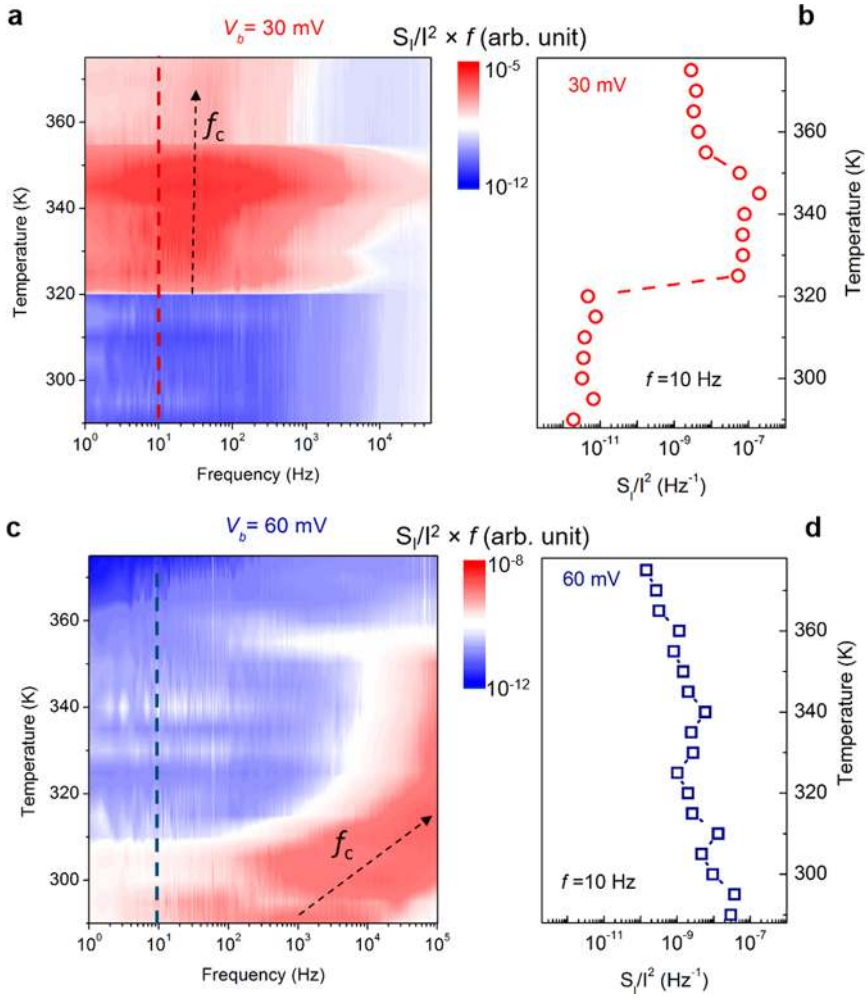

Figure 4. (a) Color map of the frequency normalized noise spectral density $S_I/I^2 \times f$ at V_b = 30 mV. The evolution of noise from $1/f$ dependence to Lorentzian at ∼320 K is seen as a change of color from blue to red. (b) The noise level profile at 10 Hz for V_b = 30 mV. Upon the appearance of Lorentzian noise, S_I/I^2 increases by four orders-of-magnitude and continues to increase toward the NC−IC transition point. Above 355 K, where the NC−IC transition occurs, the noise level sharply decreases. (c) Color map of $S_I/I^2 \times f$ at V_b = 60 mV. (d) The noise profile at 10 Hz for V_b = 60 mV. The noise level decreases with temperature as the Lorentzian moves to higher frequencies.

DOI: 10.1021/acs.nanolett.8b00729
Nano Lett. 2018, 18, 3630−3636

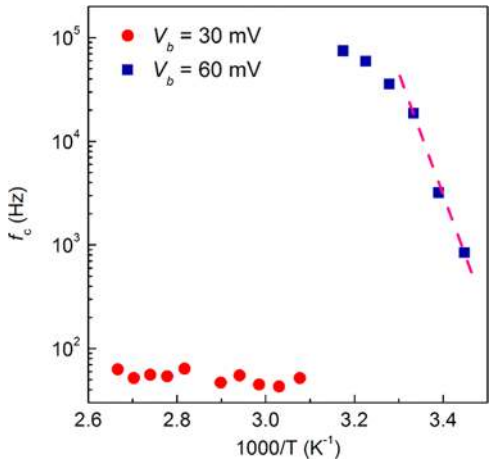

Figure 5. Lorentzian corner frequency as a function of inverse temperature. For V_b = 30 mV, f_c is in the range of 43 Hz−64 Hz, and it is independent of temperature. For V_b = 60 mV, f_c increases with temperature extremely fast. The dashed line shows the fitting used to extract the corresponding activation energy.

electric field, by confirming that the Joule heating was negligible in these experiments (Supporting Information). The temperature dependence of f_c in semiconductors is often exponential, allowing for extraction of the activation energy, E_a, of traps responsible for G-R noise.[22,25,26] Using the data for V_b = 60 mV in Figure 5, which correspond to the sliding-wave regime, one can extract $E_a \approx 2.3$ eV. This energy is unrealistically high (larger than the bandgap in many semiconductors) to be compatible with a conventional G-R mechanism.[22] The bandgap of the C-CDW domains is about 0.2−0.4 eV,[7] much smaller than the extracted E_a. Thus, LFN in this material system has a unique origin associated with the certain domains in NC-CDW phase and their evolution under electric and temperature stimuli.

Systems that contain few fluctuators demonstrate random telegraph signal (RTS) noise. RTS noise with Lorentzian spectrum has been observed in many nanoscale devices,[25,26] and it also has been encountered in bulk quasi-1D CDW systems.[2,3] We performed time-domain measurements for V_b between 100 and 121 mV, where 1*T*-TaS_2 device started to show Lorentzian spectrum (Figure 6a). At V_b = 100 mV, only "tails" with $1/f^2$-dependence could be recorder because f_c was below the measurement range. We found that at these biases, 1*T*-TaS_2 reveal large levels of the multistate RTS noise. Figure 6b−d show the RTS noise at different time scales as V_b increases from 100 to 121 mV. The occurrence of RTS noise indicates that depinning takes place in just a few domains. Interestingly, a very small V_b increase from 100 to 106 mV (Figure 6b) leads to a significant change in the current fluctuations. The amplitude of the pulses increases and the number of levels becomes greater than three, meaning that the number of depinned domains increases sharply with increasing bias. This scenario is drastically different from classical RTS noise in semiconductor devices where biasing conditions usually change the pulses duration and intervals between pulses but not the amplitude or number of levels.[19,25,26]

If we consider a shorter time scale, the traces for the same bias, V_b = 106 mV, again look like two- or three-level RTS

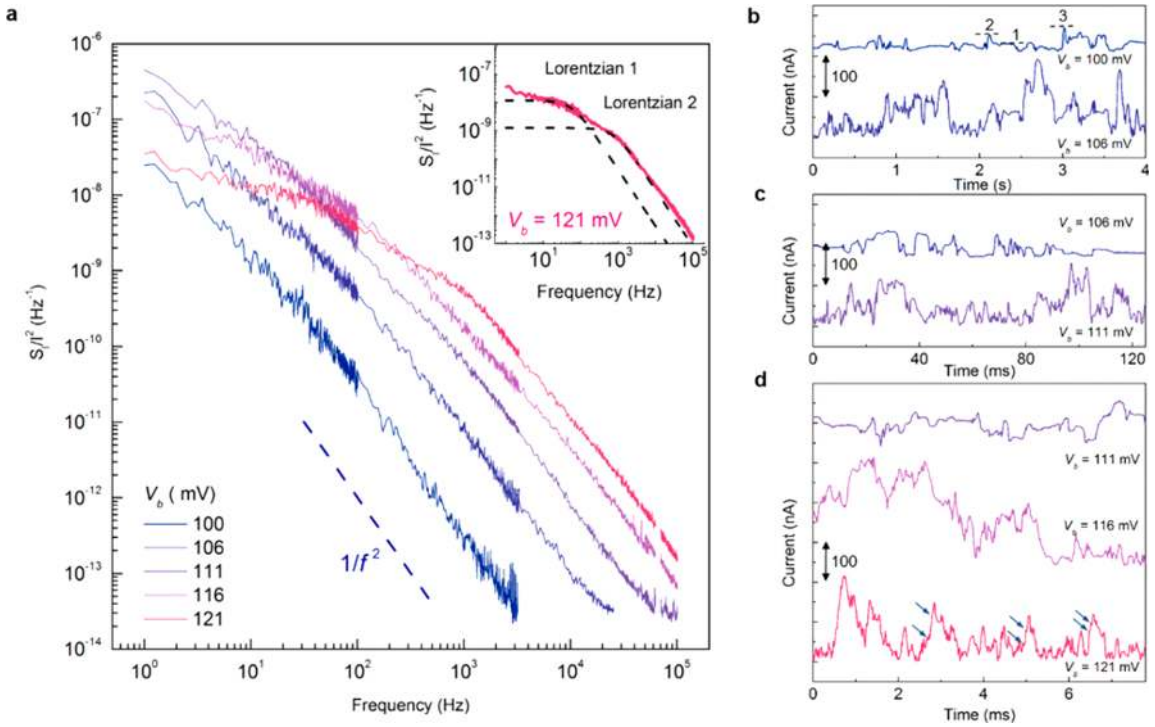

Figure 6. (a) The noise spectral density after onset of sliding at different V_b. The spectra show "tails" of the Lorentzian noise with $1/f^2$dependence at V_b = 100 mV. The corner frequency increases with increasing V_b. Inset shows that at some biasing condition, for example, V_b = 121 mV, the spectrum can be fitted better with two Lorentzian spectra with different f_c, in line with the RTS noise model. (b−d) Time-domain signals at V_b and time scales. Numbers 1, 2, and 3 indicate three characteristic levels contributing to RTN. Note that a small increase of the bias results in a significant change in the noise. The amplitude of the pulses increases and number of fluctuators becomes larger. This is different from classical RTS noise in semiconductor devices.

DOI: 10.1021/acs.nanolett.8b00729
Nano Lett. 2018, 18, 3630−3636

(Figure 6c). This is because at a short time scale the rare high-amplitude events are not captured. A small increase in V_b results in the same changes, however. The time traces for further-reduced time scales show a consistent trend (Figure 6d). The bias voltage increases the number of RTS levels, that is, discrete fluctuators. At V_b = 116 and 121 mV, the time traces in this time scale are not standard RTS because there are too many levels (Figure 6d). However, the noise is still non-Gaussian because the time traces are highly asymmetric.[19,25,26] For V_b = 121 mV, the high amplitude peaks can only be attained after a series of pulses with smaller amplitudes. This suggests that V_b changes the number of discrete fluctuators and these fluctuators are not independent. One can associate the fluctuators with certain domains in the NC-CDW phase and then consider the LFN to be the result of the random processes of the wave depinning from various domains and domain interactions. This explains the extremely strong dependence of noise on V_b and T. Depinning of a domain lowers the depinning energy of neighboring domains due to their interaction. As a result, the overall activation energy decreases with the increasing number of depinned islands and leads to the observed extremely strong noise dependence on V_b and T.

The lower bound of the size of the fluctuators can be roughly estimated by assuming that current fluctuations are due to switching between pinned and depinned states within a given domain area in a single layer. In this case, the change in the current, δI, is defined by the change in the conducting volume, ΔV, $\Delta V/V = \delta I/I$. Here $V = \Omega\zeta N$ is the sample volume, Ω is the sample area, ζ is the layer thickness, N is the number of layers, $\Delta V = \Delta\Omega\zeta$, and $\Delta\Omega$ is the domain area). If due to the depinning event, I, changes by δI, and taking the smallest current step $\delta I \approx 5-10$ nA (see Figure 6d), we obtain $(\Delta\Omega)^{1/2} = (\Omega N \delta I/I)^{1/2} \sim 20-30$ nm. This value is several times larger than the C-CDW domain sizes determined by scanning tunneling microscopy.[12] Although at this point, it is not possible to explain the exact nature of the fluctuators; one can assume that they are associated with the groups of C-CDW domains, IC-CDW phase between the C-CDW islands, coherent regions of the NC-CDW phase, as well as the system switching between the CDW phases.

In summary, we demonstrated CDW sliding in an archetypical 2D material via measurements of the low-frequency current fluctuations. The electronic noise in 1T-TaS_2 devices has two pronounced maxima at the bias voltages, which correspond to the onset of CDW sliding and the NC-to-IC phase transition. The main discovery is that noise in 2D CDW systems has unique physical origin associated with evolution and interaction of relatively large discrete fluctuators. The LFN spectroscopy provides new insights on transport phenomena in this mixed phase. Considering that many 2D materials undergo transitions to various CDW phases near RT, the results are important not only for understanding the CDW physics but also for future device applications of these materials.

Methods. *1T-TaS_2 Crystal Growth.* The source 1T-TaS_2 crystals were grown by chemical vapor transport, where the 1T polytype was isolated by fast quenching from the crystal growth temperature. Elemental tantalum (20.4 mmol, Sigma-Aldrich 99.99% purity) and sulfur (41.1 mmol, J.T. Baker >99.9% purity) were ground with mortar/pestle and placed in a 17.8 × 1.0 cm fused quartz ampule (cleaned overnight with nitric acid followed by 24 h anneal at 900 °C). Elemental iodine (J.T. Baker 99.9% purity) was added (~65 mg for a ~ 14.0 cm^3 ampule volume). The ampule was evacuated and backfilled three times with argon with cooling to mitigate I_2 sublimation. Next the ampule was flame-sealed and heated in a two-zone tube furnace at 10 °C min^{-1} to 975 °C (hot zone) and 875 °C (cool zone). These temperatures were held for 1 week. Then the ampule was removed from the hot furnace and immediately quenched in a water−ice−NaCl bath. The structure and phase purity were verified by powder X-ray diffraction, and the stoichiometry was confirmed with energy dispersive spectroscopy and electron-probe microanalysis (Supporting Information).

Device Fabrication. 1T-TaS_2 thin films were mechanically exfoliated from the bulk crystals and deposited on the Si/SiO_2 substrate. To protect the 1T-TaS_2 thin film from oxidation in air, we used h-BN capping immediately after the exfoliation. A thin film of h-BN was aligned and transferred on top of 1T-TaS_2 layer by the dry transfer method. To fabricate 1T-TaS_2 devices, we used electron beam lithography for defining the electrodes. The channel length was in the range of 1−3 μm, and the width was in the range of 0.8−1.5 μm. We used reactive ion etching to remove part of the h-BN capping layer, and deposit metal for forming edge contacts with the 1T-TaS_2 channel. The electrode materials were 10 nm Ti and 100 nm Au.

Electronic Noise Measurements. The noise spectra were measured with a dynamic signal analyzer (Stanford Research 785) after the signal was amplified by low-noise amplifier (Stanford Research 560). To minimize the 60 Hz noise and its harmonics, we used a battery biasing circuit to apply voltage bias to the devices. The devices were connected with the Lakeshore cryogenic probe station TTPX. All $I-V$ characteristics were measured in the cryogenic probe station (Lakeshore TTPX) with a semiconductor analyzer (Agilent B1500). The time domain RTS signals were acquired with the same equipment. In the noise spectra, we removed the data that corresponds to the noise floor of the measurement setup and the 60-Hz electrical grid, if there were any. The noise measurements were conducted in the two-terminal device configuration. Because the contact resistance was negligibly small compared to the channel resistance (Figure S4), the measured noise response is dominated by the channel. More details about the noise measurements can be found in the Supporting Information.

■ ASSOCIATED CONTENT

Supporting Information

The Supporting Information is available free of charge on the ACS Publications website at DOI: 10.1021/acs.nanolett.8b00729.

Material synthesis and characterization; device $I-V$ characteristics and onset of CDW sliding; noise spectroscopy as a characterization method for quasi-2D CDW sliding; noise measurements and data processing; estimation of temperature rise in 1T-TaS_2 devices; contact resistance of quasi-2D 1T-TaS_2 devices; additional figures and references (PDF)

■ AUTHOR INFORMATION

Corresponding Author

*E-mail: balandin@ece.ucr.edu; http://balandingroup.ucr.edu/.

ORCID

Guanxiong Liu: 0000-0001-8695-8671

Tina T. Salguero: 0000-0001-9396-3583

DOI: 10.1021/acs.nanolett.8b00729
Nano Lett. 2018, 18, 3630−3636

Author Contributions

A.A.B. conceived the idea, coordinated the project, and led the experimental data analysis; G.L. designed the experiments, fabricated the devices, conducted noise measurements, and performed experimental data analysis; S.R. performed electronic noise data analysis; T.T.S. supervised material synthesis and contributed to materials characterization; M.A.B. synthesized 1*T*-TaS_2 crystals and performed materials characterization. All authors contributed to the manuscript preparation.

Notes

The authors declare no competing financial interest.

■ ACKNOWLEDGMENTS

This work was supported in part by the National Science Foundation (NSF) Emerging Frontiers of Research Initiative (EFRI) 2-DARE project "Novel Switching Phenomena in Atomic MX_2 Heterostructures for Multifunctional Applications" (NSF EFRI-1433395); Semiconductor Research Corporation (SRC) and the Defense Advanced Research Project Agency (DARPA) through the STARnet Center for Function Accelerated nano-Material Engineering (FAME); and the University of California − National Laboratory Collaborative Research and Training Program (UC-NL CRT) project "Mesoscopic Two-Dimensional Materials: From Many-Body Interactions to Device Applications".

■ REFERENCES

(1) Grüner, G. The Dynamics of Charge-Density Waves. *Rev. Mod. Phys.* **1988**, *60* (4), 1129−1181.
(2) Bloom, I.; Marley, A. C.; Weissman, M. B. Nonequilibrium Dynamics of Discrete Fluctuators in Charge-Density Waves in $NbSe_3$. *Phys. Rev. Lett.* **1993**, *71* (26), 4385−4388.
(3) Bloom, I.; Marley, A. C.; Weissman, M. B. Discrete Fluctuators and Broadband Noise in the Charge-Density Wave in NbSe3. *Phys. Rev. B: Condens. Matter Mater. Phys.* **1994**, *50* (8), 5081−5088.
(4) Grüner, G.; Zawadowski, A.; Chaikin, P. M. Nonlinear Conductivity and Noise due to Charge-Density-Wave Depinning in $NbSe_3$. *Phys. Rev. Lett.* **1981**, *46* (7), 511−515.
(5) Bhattacharya, S.; Stokes, J. P.; Robbins, M. O.; Klemm, R. A. Origin of Broadband Noise in Charge-Density-Wave Conductors. *Phys. Rev. Lett.* **1985**, *54* (22), 2453−2456.
(6) Jamet, J. P.; Bouchiat, H.; Dumas, J.; Schlenker, C. Broad-Band 1/f Noise and Nonlinear Conductivity in an Insulating Charge-Density Wave System at Low Electric-Fields. *Europhys. Lett.* **1992**, *18* (3), 195−200.
(7) Sipos, B.; Kusmartseva, A. F.; Akrap, A.; Berger, H.; Forró, L.; Tutiš, E. From Mott State to Superconductivity in 1T-TaS_2. *Nat. Mater.* **2008**, *7* (12), 960−965.
(8) Joe, Y. I.; Chen, X. M.; Ghaemi, P.; Finkelstein, K. D.; De La Peña, G. A.; Gan, Y.; Lee, J. C. T.; Yuan, S.; Geck, J.; MacDougall, G. J.; et al. Emergence of Charge Density Wave Domain Walls above the Superconducting Dome in 1T-$TiSe_2$. *Nat. Phys.* **2014**, *10* (6), 421−425.
(9) Samnakay, R.; Wickramaratne, D.; Pope, T. R.; Lake, R. K.; Salguero, T. T.; Balandin, A. A. Zone-Folded Phonons and the Commensurate−incommensurate Charge-Density-Wave Transition in 1T-TaSe2 Thin Films. *Nano Lett.* **2015**, *15* (5), 2965−2973.
(10) Hollander, M. J.; Liu, Y.; Lu, W. J.; Li, L. J.; Sun, Y. P.; Robinson, J. A.; Datta, S. Electrically Driven Reversible Insulator-Metal Phase Transition in 1T-TaS_2. *Nano Lett.* **2015**, *15* (3), 1861−1866.
(11) Tsen, A. W.; Hovden, R.; Wang, D.; Kim, Y. D.; Okamoto, J.; Spoth, K. A.; Liu, Y.; Lu, W.; Sun, Y.; Hone, J. C.; et al. Structure and Control of Charge Density Waves in Two-Dimensional 1T-TaS_2. *Proc. Natl. Acad. Sci. U. S. A.* **2015**, *112* (49), 15054−15059.
(12) Ma, L.; Ye, C.; Yu, Y.; Lu, X. F.; Niu, X.; Kim, S.; Feng, D.; Son, Y.; Chen, X. H.; Zhang, Y. A Metallic Mosaic Phase and the Origin of Mott-Insulating State in 1T-TaS_2. *Nat. Commun.* **2016**, *7*, 10956.
(13) Liu, G.; Debnath, B.; Pope, T. R.; Salguero, T. T.; Lake, R. K.; Balandin, A. A. A Charge-Density-Wave Oscillator Based on an Integrated Tantalum Disulfide−boron Nitride−graphene Device Operating at Room Temperature. *Nat. Nanotechnol.* **2016**, *11* (10), 845−850.
(14) Vaskivskyi, I.; Mihailovic, I. A.; Brazovskii, S.; Gospodaric, J.; Mertelj, T.; Svetin, D.; Sutar, P.; Mihailovic, D. Fast Electronic Resistance Switching Involving Hidden Charge Density Wave States. *Nat. Commun.* **2016**, *7*, 11442.
(15) Liu, G.; Zhang, E. X.; Liang, C. D.; Bloodgood, M. A.; Salguero, T. T.; Fleetwood, D. M.; Balandin, A. A. Total-Ionizing-Dose Effects on Threshold Switching in 1T-TaS2 Charge Density Wave Devices. *IEEE Electron Device Lett.* **2017**, *38* (12), 1724−1727.
(16) DiSalvo, F. J.; Fleming, R. M. Search for a Sliding Charge Density Wave in Layered Compounds. *Solid State Commun.* **1980**, *35*, 685−687.
(17) Sinchenko, A. A.; Lejay, P.; Monceau, P. Sliding Charge-Density Wave in Two-Dimensional Rare-Earth Tellurides. *Phys. Rev. B: Condens. Matter Mater. Phys.* **2012**, *85*, 1−5.
(18) Dutta, P.; Horn, P. M. Low-Frequency Fluctuation in Solids: 1/f Noise. *Rev. Mod. Phys.* **1981**, *53* (3), 497−516.
(19) Fleetwood, D. M. 1/f Noise and Defects in Microelectronic Materials and Devices. *IEEE Trans. Nucl. Sci.* **2015**, *62* (4), 1462−1486.
(20) Cox, S.; Singleton, J.; McDonald, R. D.; Migliori, A.; Littlewood, P. B. Sliding Charge-Density Wave in Manganites. *Nat. Mater.* **2008**, *7* (1), 25−30.
(21) Kundu, H. K.; Ray, S.; Dolui, K.; Bagwe, V.; Choudhury, P. R.; Krupanidhi, S. B.; Das, T.; Raychaudhuri, P.; Bid, A. Quantum Phase Transition in Few-Layer NbSe2 Probed through Quantized Conductance Fluctuations. *Phys. Rev. Lett.* **2017**, *119* (22), 226802−1.
(22) Mitin, V.; Reggiani, L.; Varani, L. Generation-Recombination Noise in Semiconductors. In *Noise and fluctuation control in electronic devices*; Balandin, A. A., Ed.; American Scientific Publishers: Los Angeles, 2002; pp 11−29.
(23) Topalian, Z.; Li, S.; Niklasson, G. A.; Granqvist, C. G.; Kish, L. B. Resistance Noise at the Metal − Insulator Transition in Thermochromic VO_2 Films. *J. Appl. Phys.* **2015**, *117* (2), 025303.
(24) Kawasaki, M.; Chaudhari, P.; Gupta, A. 1/f Noise in $YBa_2Cu_2O_{7-Z}$ Superconducting Bicrystal Grain-Boundary Junctions. *Phys. Rev. Lett.* **1992**, *68* (7), 1065−1068.
(25) Çelik-Butler, Z.; Vasina, P.; Amarasinghe, N. V. A Method for Locating the Position of Oxide Traps Responsible for Random Telegraph Signals in Submicron MOSFET's. *IEEE Trans. Electron Devices* **2000**, *47* (3), 646−648.
(26) Kirton, M. J.; Uren, M. J. Noise in Solid-State Microstructures: A New Perspective on Individual Defects, Interface States and Low-Frequency (1/f) Noise. *Adv. Phys.* **1989**, *38* (4), 367−468.

DOI: 10.1021/acs.nanolett.8b00729
Nano Lett. 2018, 18, 3630−3636